Pergamon

Int. J. Solids Structures Vol. 32, No. 15, pp. 2257–2278, 1995

0020–7683/95 $9.50 + .00

0020–7683(94)00227–4

BOUNDARY ELEMENT METHOD FOR DYNAMIC POROELASTIC AND THERMOELASTIC ANALYSES

J. CHEN† and G. F. DARGUSH
Department of Civil Engineering, State University of New York at Buffalo, Buffalo, NY 14260, U.S.A.

(*Received* 9 *September* 1993; *in revised form* 7 *September* 1994)

Abstract—A boundary element method is developed for transient and time harmonic analysis of problems in dynamic poroelasticity and generalized thermoelasticity, involving both two- and three-dimensional geometries. Laplace domain infinite space fundamental solutions are employed to produce a formulation that requires only surface discretization. Consequently, the resulting algorithm provides an attractive alternative to existing volume-based methods, particularly for media of infinite extent. Details of the formulation and numerical implementation are presented. Several applications are included to validate the method and to emphasize certain aspects of the dynamic theory.

INTRODUCTION

In recent years, there has been an increasing interest in physical phenomena that can be modeled by the dynamic theories of poroelasticity and thermoelasticity. For example, poroelastic analysis is applicable in seismology, foundation design, and in the study of wave propagation in wet bones. Meanwhile, dynamic thermoelasticity is relevant for problems in aerospace engineering involving high heat flux. More contemporary applications include the areas of superconductivity and laser technology. Despite this diversity, the two theories are completely analogous due to a common underlying thermodynamics. In a series of remarkable papers, Biot developed the theoretical basis for both disciplines and established the analogy.

The first model of dynamic poroelasticity, which pioneered the theory of wave propagation in fluid-saturated porous media, was developed in an intuitive manner by Biot (1956a,b; 1962a,b). Its essential correctness has been confirmed both from a two-scaled analysis of the Navier–Stokes equations (Burridge and Keller, 1981) and from the viewpoint of the theory of mixtures (Bowen, 1982). The theory has also been verified by experimental observations (e.g. Plona, 1980).

Information concerning classical dynamic thermoelasticity can be found in the works of Biot (1956c), Chadwick (1960), and Nowacki (1975). Since the classical theory implies an infinite propagation speed for thermoelastic disturbances, which is not acceptable from a physical point of view, nonclassical (or generalized) thermoelastic theories (e.g. Lord and Schulman, 1967; Green and Lindsay, 1972) aimed at eliminating the paradox have appeared in the technical literature.

The complexity of the governing equations, which couple the behavior of a vector displacement field with that of a scalar pressure (or temperature) field, precludes the derivation of analytical solutions for all but the simplest of problems. More generally, numerical methods must be employed. Domain-based approaches, particularly those involving the finite element method, have been developed and applied with some success (Zienkiewicz *et al.*, 1980; Zienkiewicz and Shiomi, 1984; Prevost and Tao, 1983). However, these problems invariably involve wave propagation, often in media of infinite extent. In such cases, special techniques are required for wave front tracking and radiation boundary condition specification. On the other hand, a boundary element approach could be very attractive for these problems, at least for those involving piecewise homogeneous media.

† Present address: STV Group/Seelye Stevenson Value & Knecht, Inc., 225 Park Ave. South, New York, NY 10003-1604, U.S.A.

Initially the development of the boundary element method (BEM) for poroelasticity was limited to quasistatic problems. Noteworthy publications include those by Cleary (1977), Banerjee and Butterfield (1981), and Cheng and Liggett (1984). Time-domain, boundary-only solutions were provided by Nishimura and Kobayashi (1989) and Dargush and Banerjee (1989a). In the realm of dynamic poroelasticity, the BEM integral representations presented by Predeleanu (1984) and Manolis and Beskos (1989) are written as six equations with six unknowns (e.g. displacement of solid skeleton u_i and average displacement of fluid relative to the solid w_i). The fundamental solutions for the above-mentioned equations were obtained by Manolis and Beskos (1989) in the Laplace transform domain and by Norris (1985) in the frequency domain. Unfortunately these formulations are not satisfactory, since Bonnet (1987) and Boutin *et al.* (1987) have shown that only four quantities (e.g. solid displacements and fluid pressure) are independent variables for poroelastic problems. More recently, Cheng and Badmus (1991) and Dominguez (1992) developed frequency domain boundary element methods for dynamic poroelasticity in terms of independent variables. Both papers contain numerical implementations and applications, which are limited in scope to two-dimensional time-harmonic problems.

Time-domain BEM solutions to quasistatic thermoelastic problems were first provided in Dargush and Banerjee (1989b; 1990). In the realm of classical dynamic thermoelasticity, the well-known fundamental solution in the transform domain by Nowacki (1964) and the reciprocal theorem by Ionescu-Cazimir (1964) have been available for a long time. On the other hand, several authors (e.g. Sladek and Sladek, 1984) have written out various forms of fundamental solution and integral representation for the classical theory, but no BEM application has been reported to verify the validity of these formulations. Furthermore, nothing has appeared concerning generalized thermoelasticity.

In the present work, a single BEM is developed for application to dynamic poroelasticity, classical thermoelasticity, and nonclassical thermoelasticity by extending the Biot analogy. The resulting integral representation is written in the Laplace transform domain in terms of independent variables. The numerical implementation utilizes a collocation-based conforming element approach, featuring adaptive integration strategies. This permits direct solution of time-harmonic problems in the frequency domain. More importantly, with the application of a robust numerical inversion algorithm, accurate transient solutions are obtained while maintaining a boundary-only formulation. It appears that this has not been accomplished previously for dynamical problems in either poroelasticity or thermoelasticity. Furthermore, both two- and three-dimensional domains are considered throughout.

The following section begins with a presentation of the governing differential equations for the relevant poroelastic and thermoelastic theories. These equations are consolidated into a generalized set by defining the poro–thermo analogy in the Laplace transform domain. A boundary integral representation is developed directly from those equations by employing infinite space fundamental solutions. Then, aspects of a numerical implementation are discussed. As noted above, this implementation permits the solution of transient or time-harmonic problems, while requiring only surface discretization. The entire methodology is validated through a series of numerical examples, including applications to underground explosions and foundation impedance. For completeness, the required Laplace domain kernel functions are detailed in the Appendix for the three-dimensional case. Subscript notation is used throughout. Thus, summations are implied by repeated subscripts, commas represent differentiation with respect to spatial coordinates, and a superposed dot denotes a partial time derivative.

GOVERNING EQUATIONS

Dynamic poroelasticity

Biot's equations governing the behavior of a poroelastic medium can be written, following Zienkiewicz *et al.* (1980), in cartesian form:

$$\sigma_{ij} = \lambda u_{k,k}\delta_{ij} + \mu(u_{i,j} + u_{j,i}) - \alpha p\delta_{ij}, \tag{1a}$$

$$\theta = \alpha u_{k,k} + \frac{1}{Q}p, \tag{1b}$$

$$\sigma_{ij,j} + f_i = \rho\ddot{u}_i + \rho_f\ddot{w}_i, \tag{1c}$$

$$q_i = -\kappa(p_{,i} + \rho_f\ddot{u}_i + m\ddot{w}_i), \tag{1d}$$

$$\dot{\theta} + q_{i,i} = \psi. \tag{1e}$$

These represent the first and second constitutive relations, the momentum balance equations, generalized Darcy's law, and the continuity equation, respectively. The subscript i, $j = 1, 2, 3$; σ_{ij} is the total stress; p denotes the excessive fluid pore pressure (pressure is taken as positive); u_i is the displacement of the solid skeleton; w_i denotes the average displacements of the fluid relative to the solid; and θ represents the increment of fluid content. Additionally, the relationship between the fluid volume flux vector q_i and average velocity of fluid relative to the solid $\dot{w}_i$ can be defined as $q_i = \dot{w}_i$. The elastic constants λ and μ are termed drained Lamé constants, $\kappa = k/\eta$ is the permeability coefficient, while η and k denote the fluid viscosity and the specific permeability, respectively. The quantities ρ_s and ρ_f represent the solid and fluid density, while $\rho = (1-n)\rho_s + n\rho_f$ is the density of the solid–fluid mixture with n denoting porosity. Meanwhile, ψ and f_i are the volumetric body source rate and the body force, respectively. In addition α and Q are Biot's parameters accounting for compressibility in the two-phase material. The parameter m, appearing in the generalized Darcy's law, pertains to fluid inertial effects. Zienkiewicz and Shiomi (1984) set $m = \rho_f/n$ due to a lack of experimental data to justify otherwise. Alternatively, homogenization theory can be used to establish appropriate values for m or to define an equivalent frequency-dependent permeability κ (Auriault *et al.*, 1985).

It is not possible to rewrite eqn (1) in the time domain only in terms of the independent variables u_i and p without increasing the order of the resulting differential equations. However, the above task can be accomplished in the transform domain by first taking the Laplace transform of eqn (1). After some further manipulation, the governing equations representing the balance of momentum and mass can be written as

$$\mu\tilde{u}_{i,jj} + (\lambda+\mu)\tilde{u}_{j,ij} - \rho_1 s^2\tilde{u}_i - \alpha_1\tilde{p}_{,i} + \tilde{f}_i = 0, \tag{2a}$$

$$\zeta\tilde{p}_{,ii} - \frac{s}{Q}\tilde{p} - \alpha_2 s\tilde{u}_{i,i} + \tilde{\psi} = 0, \tag{2b}$$

where Latin subscripts assume the values 1, 2, 3, the tilde denotes the Laplace transformation, $\alpha_1 = \alpha - \rho_f s\zeta$, $\alpha_2 = \alpha - \rho_f s\zeta$, $\rho_1 = \rho - \rho_f^2 s\zeta$, $\zeta = (1/\kappa + ms)^{-1}$ and s is the Laplace transform parameter. (Separate parameters α_1 and α_2 have been introduced in eqns (2a,b) to represent the same function in order to extend the work to dynamic thermoelasticity.) Notice that the effective permeability ζ is now a complex valued function of s (i.e. frequency-dependent). Biot (1962a,b) suggested that several material parameters present in eqn (1) should actually be replaced by integrodifferential operators. This can be readily accommodated in the Laplace transform domain form expressed in eqn (2). However, the difficulty lies in determining the appropriate operators for a particular physical problem.

Dynamic thermoelasticity

In classical thermoelasticity theory, the displacement field is governed by a wave-type equation (hyperbolic), while the temperature field is formulated on the principles of the classical theory of heat conduction and, consequently, is governed by a diffusion type equation (parabolic). As has been pointed out by many people (e.g. Vernotte, 1958), the diffusion-type equation leads to an infinite propagation velocity for a finite thermal impulse, a physically unacceptable situation. This behavior has provided reason to doubt the validity

of Fourier's law for initial value problems at short times. Thus, modified dynamic thermoelasticity theories have been proposed that involve hyperbolic-type heat transport equations and allow for so-called 'second sound' effects. In 1967, Lord and Shulman (L–S) proposed a new theory by incorporating a flux rate with one relaxation time, τ_0, into Fourier's law. Through this relationship the temperature distribution is governed by a partial differential equation of the hyperbolic type, and heat conduction will be described as a wave propagation phenomenon. In 1972, Green and Lindsay (G–L), by introducing two relaxation times τ_1 and τ_2 for the thermoelastic process, formulated an alternative generalized theory of dynamic thermoelasticity with a second scalar wave, which is based on an entropy production inequality. Contrary to L–S theory, the G–L theory does not violate Fourier's law when the solid has a center of symmetry.

One can write the basic equations for linearized thermoelasticity expressing, respectively, the first constitutive relationship, the second constitutive relationship (for the entropy), the equations of motion, Fourier's law of heat conduction, and the linearized entropy balance equation, as

$$\sigma_{ij} = \lambda u_{k,k}\delta_{ij} + \mu(u_{i,j} + u_{j,i}) - \beta(T + \tau_1 \dot{T})\delta_{ij}, \tag{3a}$$

$$T_0 S = \beta T_0 u_{k,k} + c_\varepsilon (T + \tau_2 \dot{T}), \tag{3b}$$

$$\sigma_{ij,j} + f_i = \rho \ddot{u}_i, \tag{3c}$$

$$q_i + \tau_0 \dot{q}_i = -\kappa T_{,i}, \tag{3d}$$

$$T_0 \dot{S} + q_{i,i} = \psi, \tag{3e}$$

where $c_\varepsilon = \rho c$, $\beta = (3\lambda + 2\mu)\alpha_\varepsilon$, λ and μ are the Lamé constants, u_i, σ_{ij}, T_0, T, q_i, f_i and ψ are the displacement, stress, reference temperature, temperature difference, heat flux, body force, and heat source, respectively. Meanwhile, ρ, β, α_ε, κ, c_ε, and c are the density, stress–temperature modulus, the coefficient of linear volume expansion, conductivity, specific heat at constant strain, and specific heat referred to the unit mass of the body, respectively. The quantity S is the entropy per unit volume and unit time.

The relaxation parameters τ_0, τ_1, τ_2 govern various dynamic thermoelastic models. When $\tau_0 = \tau_1 = \tau_2 = 0$, eqns (3) reduce to the Classical Theory (Nowacki, 1986). When only $\tau_1 = \tau_2 = 0$, eqns (3) reduce to the L–S theory (Lord and Shulman, 1967), where Fourier's law of heat conduction, eqn (3d), is modified by the introduction of the relaxation time τ_0, which represents a finite building time for the onset of a heat flow after a temperature gradient is suddenly applied. Conversely, if a thermal gradient is suddenly removed, there is a lag in the disappearence of the heat flow. When only $\tau_0 = 0$, eqns (3) reduce to the G–L theory (Green and Lindsay, 1972), where two relaxation times τ_1, τ_2 are introduced by modifying the Duhamel–Neumann relationships (3a) and the entropy density relationships (3b).

Eliminating $T_0\dot{S}$ and q_i from eqns (3b,d,e) and σ_{ij} from eqns (3a,c), we obtain the following motion and energy equations in the time domain:

$$\mu u_{i,jj} + (\lambda + \mu) u_{j,ji} - \rho \ddot{u}_i - \beta(T_{,i} + \tau_1 \dot{T}_{,i}) + f_i = 0, \tag{4a}$$

$$\kappa T_{,jj} - c_\varepsilon(\dot{T} + (\tau_0 + \tau_2)\ddot{T}) - \beta T_0(\dot{u}_{i,i} + \tau_0 \ddot{u}_{i,i}) + \psi = 0. \tag{4b}$$

Application of the Laplace transform to eqns (4a,b) yields

$$\mu \tilde{u}_{i,jj} + (\lambda + \mu)\tilde{u}_{j,ji} - \rho s^2 \tilde{u}_i - \beta(1 + \tau_1 s)\tilde{T}_{,i} + \tilde{f}_i = 0, \tag{5a}$$

$$\zeta_t \tilde{T}_{,ii} - c_\varepsilon \left(1 + \frac{\tau_2 s}{1 + \tau_0 s}\right) s\tilde{T} - \beta T_0 s \tilde{u}_{j,j} + \tilde{\psi} = 0, \tag{5b}$$

where

$$\zeta_t = \frac{\kappa}{1+\tau_0 s}.$$

Poro–thermo analogy

As first indicated by Biot (1956c), the processes involved in poroelastic and thermoelastic deformation have much in common, from a thermodynamic standpoint. This is manifested in the similarity of eqns (1) and (3) in the time domain, and (2) and (5) in the transform domain. Comparison of the latter set, involving independent variables, is most relevant for our development. With that in mind, we construct the following set of coupled differential equations governing the dynamic behavior of poroelastic and thermoelastic media:

$$\mu\tilde{u}_{i,jj} + (\lambda+\mu)\tilde{u}_{j,ji} - \rho_1 s^2 \tilde{u}_i - \alpha_1 \tilde{\Theta}_{,i} + \tilde{f}_i = 0, \tag{6a}$$

$$\zeta\tilde{\Theta}_{,ii} - \frac{1}{M} s\tilde{\Theta} - \alpha_2 s\tilde{u}_{i,i} + \tilde{\psi} = 0, \tag{6b}$$

in the Laplace transform domain. In the above, $\tilde{u}_i$ represents the displacement, while $\tilde{\Theta}$ is the excess pore pressure in poroelasticity or the temperature difference in thermoelasticity. Additionally, λ and μ are the Lamé constants, $\tilde{f}_i$ and $\tilde{\psi}$ represent body forces and sources, respectively. The remaining parameters are defined as follows:

$$\zeta = \frac{1}{1/\kappa + ms}, \tag{7a}$$

$$\rho_1 = \rho - \rho_f^2 s\zeta, \tag{7b}$$

$$\alpha_1 = \alpha(1+\tau_1 s) - \rho_f s\zeta, \tag{7c}$$

$$\alpha_2 = \alpha T_0 - \rho_f s\zeta, \tag{7d}$$

$$\frac{1}{M} = \frac{1+\tau_2 s}{Q}. \tag{7e}$$

For poroelasticity, κ, ρ_f, ρ, and n are the permeability, fluid density, two-phase material density, and porosity, respectively, with $m = \rho_f/n$ as in Zienkiewicz and Shiomi (1984). The remaining active parameters α and Q account for the compressibility of the two-phase material. The dummy parameters τ_1, τ_2, and T_0 assume the values 0, 0, and 1, respectively. Consequently, $\alpha_1 = \alpha_2$ and $M = Q$.

Meanwhile, in thermoelasticity, κ, ρ, T_0, c_ε and α_ε represent the thermal conductivity, density, reference temperature, specific heat at constant strain, and the coefficient of thermal expansion, respectively, with $Q = 1/c_\varepsilon$ and $\alpha = (3\lambda+2\mu)\alpha_\varepsilon$. The inactive parameter $\rho_f = 0$. For classical thermoelasticity theory, there are no relaxation times. Therefore, the parameters τ_1 and τ_2, along with m, are all zero. The Lord–Schulman theory contains one relaxation time τ_0, where $m = \tau_0/\kappa$. Once again τ_1 and τ_2 are zero. Finally, in the Green–Lindsay theory the relaxation times τ_1 and τ_2 are active, while $m = 0$. The complete analogy is summarized in Table 1.

Boundary integral representation

Let $\tilde{B}_{\gamma\alpha}$ represent the transformed differential operator specified in eqn (6) with Greek indices assuming values 1,2,3,4. With this notation, eqn (6) can be rewritten

$$\tilde{B}_{\gamma\alpha}\tilde{u}_\alpha + \tilde{f}_\gamma = 0, \tag{8}$$

in which

Table 1. Poroelastic–thermoelastic analogy in Laplace transform domain

Poroelasticity	Classical theory	L–S theory	G–L theory
$\tilde{u}_i$	$\tilde{u}_i$	$\tilde{u}_i$	$\tilde{u}_i$
$\tilde{p}$	$\tilde{T}$	$\tilde{T}$	$\tilde{T}$
$\tilde{\sigma}_{ij}$	$\tilde{\sigma}_{ij}$	$\tilde{\sigma}_{ij}$	$\tilde{\sigma}_{ij}$
$\tilde{q}_i$	$\tilde{q}_i$	$\tilde{q}_i$	$\tilde{q}_i$
$\tilde{\theta}$	$T_0\tilde{S}$	$T_0\tilde{S}$	$T_0\tilde{S}$
$\tilde{f}_i$	$\tilde{f}_i$	$\tilde{f}_i$	$\tilde{f}_i$
$\tilde{\psi}$	$\tilde{\psi}$	$\tilde{\psi}$	$\tilde{\psi}$
α†	β	β	$\beta(1+\tau_1 s)$
α‡	βT_0	βT_0	βT_0
κ	κ	κ	κ
λ	λ	λ	λ
μ	μ	μ	μ
ρ	ρ	ρ	ρ
ρ_f	0.0	0.0	0.0
m	0.0	τ_0/κ	0.0
$1/Q$	c_v	c_v	$c_v(1+\tau_2 s)$

†In equation of motion, i.e. $\alpha = \alpha_1$.
‡In energy equation, i.e. $\alpha = \alpha_2$.

$$\tilde{u}_\alpha = (\tilde{u}_1, \tilde{u}_2, \tilde{u}_3, \tilde{\Theta})^{\mathrm{T}}, \tag{9a}$$

$$\tilde{f}_\gamma = (\tilde{f}_1, \tilde{f}_2, \tilde{f}_3, \tilde{\psi})^{\mathrm{T}}. \tag{9b}$$

Furthermore, let $\tilde{G}_{\alpha\beta}(x, \xi; s)$ and $\tilde{G}^*_{\alpha\beta}(x, \xi; s)$ represent the corresponding fundamental solution and adjoint fundamental solution, respectively, implying that

$$\tilde{B}_{\gamma\alpha}\tilde{G}_{\alpha\beta} + \delta_{\gamma\beta}\delta(x-\xi) = 0, \tag{10a}$$

$$\tilde{B}^*_{\gamma\alpha}\tilde{G}^*_{\alpha\beta} + \delta_{\gamma\beta}\delta(x-\xi) = 0, \tag{10b}$$

with Kronecker delta function $\delta_{\gamma\beta}$, Dirac delta function $\delta(x-\xi)$, and $\tilde{B}^*_{\gamma\alpha}$ as the adjoint differential operator. In three dimensions, one finds that $\tilde{G}^*_{ij} = \tilde{G}_{ij}$, $\tilde{G}^*_{4i} = -\tilde{G}_{i4}$, $\tilde{G}^*_{i4} = -\tilde{G}_{4i}$, and $\tilde{G}^*_{44} = \tilde{G}_{44}$.

A set of integral equations for the generalized theory can then be derived in a direct manner by equating the inner product of eqn (8) and $\tilde{G}^*_{\alpha\beta}$ to a null vector, i.e.

$$\int_V (\tilde{B}_{\alpha\gamma}\tilde{u}_\gamma + \tilde{f}_\alpha)\tilde{G}^*_{\alpha\beta}\,\mathrm{d}V = 0, \tag{11}$$

where the integration is performed over the volume V. This essentially forces the error associated with the satisfaction of the governing differential equations to be orthogonal to $\tilde{G}^*_{\alpha\beta}$. Next, integration by parts is performed on the individual terms within the inner product to transfer all derivatives from $\tilde{u}_\gamma$ to $\tilde{G}^*_{\alpha\beta}$. The result can be written

$$\int_S [(\lambda\tilde{u}_{k,k} - \alpha_1\tilde{\Theta})n_i + \mu(\tilde{u}_{i,j} + \tilde{u}_{j,i})n_j]\tilde{G}^*_{i\beta}\,\mathrm{d}S(x) - \int_S \tilde{u}_i[(\lambda\tilde{G}^*_{k\beta,k} + \alpha_2 s\tilde{G}^*_{4\beta})n_i + \mu(\tilde{G}^*_{i\beta,j}$$

$$+ \tilde{G}^*_{j\beta,i})n_j]\,\mathrm{d}S(x) + \int_S \zeta[\tilde{\Theta}_{,j}n_j\tilde{G}^*_{4\beta} - \tilde{\Theta}\tilde{G}^*_{4\beta,j}n_j]\,\mathrm{d}S(x) + \int_V (\tilde{f}_\gamma + \tilde{u}_\alpha\tilde{B}^*_{\alpha\gamma})\tilde{G}^*_{\gamma\beta}\,\mathrm{d}V(x) = 0, \tag{12}$$

in which n_j represents the outer normal to the bounding surface S. This can be simplified considerably by introducing surface tractions $\tilde{t}_i$ and normal flux $\tilde{q}$ for the generalized theory, where

$$\tilde{t}_i = [(\lambda \tilde{u}_{k,k} - \alpha(1+\tau_1 s)\tilde{\Theta})\delta_{ij} + \mu(\tilde{u}_{i,j} + \tilde{u}_{j,i})]n_j, \tag{13a}$$

$$\tilde{q} = -\zeta(\tilde{\Theta}_{,j} + \rho_f s\tilde{u}_j)n_j. \tag{13b}$$

These expressions are valid for both poroelasticity and thermoelasticity. After neglecting body forces $\tilde{f}_i$ and using eqns (10b) and (13), eqn (12) reduces to the following form:

$$C_{\alpha\beta}(\xi)\tilde{u}_\alpha(\xi, s) = \int_S [\tilde{G}^*_{\alpha\beta}(x, \xi; s)\tilde{t}_\alpha(x, s) - \tilde{F}^*_{\alpha\beta}(x, \xi; s)\tilde{u}_\alpha(x, s)]\, \mathrm{d}S(x), \tag{14}$$

where

$$\tilde{F}^*_{i\beta} = [(\lambda \tilde{G}^*_{k\beta,k} - \alpha T_0 s\tilde{G}^*_{4\beta})n_i + \mu(\tilde{G}^*_{i\beta,k} + \tilde{G}^*_{k\beta,i})n_k], \tag{15a}$$

$$\tilde{F}^*_{4\beta} = -\zeta(\tilde{G}^*_{4\beta,k} + \rho_f s\tilde{G}^*_{k\beta})n_k, \tag{15b}$$

and

$$\tilde{t}_\alpha = (\tilde{t}_1, \tilde{t}_2, \tilde{t}_3, \tilde{q})^{\mathrm{T}}. \tag{16}$$

The matrix $C_{\alpha\beta}$ depends only upon the local geometry at ξ, and reduces to a generalized delta function $\delta_{\alpha\beta}$ for ξ inside S and to $\frac{1}{2}\delta_{\alpha\beta}$ for ξ on a smooth portion of the boundary surface. The kernel functions, $\tilde{G}^*_{\alpha\beta}$ and $\tilde{F}^*_{\alpha\beta}$, required in eqn (14) are detailed in the Appendix for three-dimensional problems. The corresponding explicit form of the two-dimensional kernels can be found in Chen (1992), along with additional details concerning the derivation of the integral representation.

The kernels in eqn (14) are developed directly from Laplace domain infinite space Green's functions for Biot's complete dynamic poroelastic theory. The technique used for derivation is much the same as that employed by Boutin *et al.* (1987) for their frequency-domain solution. We include nothing here about the detailed derivation, which is discussed at length in Chen (1992). However, it should be noted that in various limiting cases, these solutions properly reduce to those of classical elastodynamics and steady-state poroelasticity. Furthermore, examination of $\tilde{G}^*_{\alpha\beta}$ in the Appendix reveals that for displacements generated by a unit force there are two compressional waves P_1 and P_2 and one shear wave S. The displacements are cylindrically symmetric around the direction of the force in the 3-D case and only plane symmetrical around that direction in the 2-D case. The contribution of the S-wave in the pressure response due to a point force is obviously zero. Also there is no shear wave in the fields of displacement and pressure, which are radiated by a fluid point source. These fields present a spherical symmetry for 3-D and a radial symmetry for 2-D cases centered on the fluid point source. In the corresponding frequency domain, λ_1 and λ_2 are the wave numbers of the slow compressional waves and fast compressional waves, respectively, while λ_3 represents the wave number of the shear waves.

It should also be noted that these kernels can be decomposed in the following manner:

$$\tilde{G}^*_{\alpha\beta}(x, \xi; s) = G_{\alpha\beta}(x, \xi) + \tilde{g}^*_{\alpha\beta}(x, \xi; s), \tag{17a}$$

$$\tilde{F}^*_{\alpha\beta}(x, \xi; s) = F_{\alpha\beta}(x, \xi) + \tilde{f}^*_{\alpha\beta}(x, \xi; s), \tag{17b}$$

where $G_{\alpha\beta}(x, \xi)$ and $F_{\alpha\beta}(x, \xi)$ are the time-independent steady-state poroelastic (or thermoelastic) kernels defined in Dargush and Banerjee (1989a; 1990). The steady-state three-dimensional kernels exhibit singular behavior as indicated below (Dargush, 1987):

$$\lim_{x \to \xi} G_{ij}(x, \xi) \propto \frac{1}{r}, \tag{18a}$$

$$\lim_{x \to \xi} G_{4j}(x, \xi) \propto \text{constant}, \tag{18b}$$

$$\lim_{x \to \xi} G_{i4}(x, \xi) \propto \text{constant}, \tag{18c}$$

$$\lim_{x \to \xi} G_{44}(x, \xi) \propto \frac{1}{r}, \tag{18d}$$

$$\lim_{x \to \xi} F_{ij}(x, \xi) \propto \frac{1}{r^2}, \tag{19a}$$

$$\lim_{x \to \xi} F_{4j}(x, \xi) \propto \frac{1}{r}, \tag{19b}$$

$$\lim_{x \to \xi} F_{i4}(x, \xi) \propto \text{constant}, \tag{19c}$$

$$\lim_{x \to \xi} F_{44}(x, \xi) \propto \frac{1}{r^2}, \tag{19d}$$

with analogous behavior associated with the two-dimensional counterparts. However, the remaining portions of the kernels, denoted by $\tilde{g}^*_{\alpha\beta}(x, \xi; s)$ and $\tilde{f}^*_{\alpha\beta}(x, \xi; s)$ in eqn (17), are completely nonsingular as $x \to \xi$.

NUMERICAL IMPLEMENTATION

In order to employ the integral formulation developed in the previous section for the solution of all but the most elementary problems, discretization of eqn (14) must be introduced in both time and space. Consider first the temporal representation utilized for analysis of time-harmonic and general transient behavior. For the time-harmonic case, one simply sets the Laplace transform parameter $s = i\omega$, where i is the imaginary unit and ω is the circular frequency of the applied boundary conditions. As a result, the kernel functions $\tilde{G}^*_{\alpha\beta}(x, \xi; \omega)$ and $\tilde{F}^*_{\alpha\beta}(x, \xi; \omega)$ are explicitly defined complex quantities, while $\tilde{u}_\alpha(x, \omega)$ and $\tilde{t}_\alpha(x, \omega)$ represent the generalized displacement and traction complex amplitudes, respectively.

There are at least two approaches available for general transient analysis. In the first approach, the Laplace inverse transform of eqn (14) is obtained directly, and then the kernels are evaluated by performing a numerical inverse Laplace transform. This is a computationally intensive approach, since the numerical inversion must be performed at each field point (ξ)–load point (x) pair. Moreover, the evaluation must be done carefully owing to the character of the kernel functions. On the other hand, with this methodology, the formulation can be employed for problems involving temporal changes in boundary condition types (e.g. from imposed displacement to applied traction conditions) and can be extended quite naturally to examine nonlinear phenomena.

The second approach involves solution of the boundary integral equations in the transform domain. Time-dependent boundary conditions are first transformed to the Laplace domain, the equations are solved independently at each of a series of values of the complex transform parameter s, and then finally the boundary solutions are transformed back to the time domain via a numerical inverse transform. This, in fact, is the usual approach taken in the boundary element literature when employing Laplace domain kernels [see e.g. Cruse and Rizzo (1968); Manolis and Beskos (1981); Cheng and Liggett (1984)], and is also adopted in the present work. The actual numerical implementation, detailed below, represents an extension of that developed by Banerjee and Ahmad (1985) for elastodynamics.

In the initial phase, boundary conditions specified in the time domain are transformed into Laplace-domain form by employing exact formulas for piecewise linear functions of time

$$F(\tau) = F_{n-1} + \frac{(F_n - F_{n-1})}{\Delta\tau}(\tau - \tau_{n-1}), \quad \text{for } \tau_{n-1} \leqslant \tau \leqslant \tau_n; n = 1, 2, \ldots, N, \tag{20}$$

where

$$F_n = F(\tau_n), \tag{21a}$$

$$\tau_n = n\Delta\tau. \tag{21b}$$

Utilizing eqn (20) in the definition of the Laplace transform

$$\tilde{F}(s) = \int_{-\infty}^{\infty} F(\tau)\, \mathrm{e}^{-s\tau}\, \mathrm{d}\tau, \tag{22}$$

produces the required result,

$$\tilde{F}(s) = \sum_{n=1}^{N} \frac{1}{s^2\Delta\tau}\{(F_n - F_{n-1})[\mathrm{e}^{-s\tau_{n-1}} - \mathrm{e}^{-s\tau_n}] + s\Delta\tau[F_{n-1}\,\mathrm{e}^{-s\tau_{n-1}} - F_n\,\mathrm{e}^{-s\tau_n}]\}. \tag{23}$$

This formula is used to calculate the quantities $\tilde{t}_\alpha(x, s)$ and $\tilde{u}_\alpha(x, s)$, appearing in eqn (14), that correspond to the specified boundary conditions.

Of course, the question remains as to the appropriate values of s at which the integral equations are to be written. These values are determined through the selection of an algorithm for Laplace transform inversion. The present work uses the Fast Laplace Inverse Transform (FLIT) method of Durbin (1974), which combines Fourier cosine and sine transforms to reduce numerical error. This formulation yields time-domain functional values

$$F(\tau_n) = \frac{2\,\mathrm{e}^{n\beta\Delta\tau}}{\tau_N}\left[-\tfrac{1}{2}\mathrm{Re}\{\tilde{F}(s_0)\} + \mathrm{Re}\left\{\sum_{k=0}^{N-1}(\tilde{A}_k + \mathrm{i}\tilde{B}_k)W^{nk}\right\}\right] \quad \text{for } n = 0, 1, \ldots, N-1 \tag{24}$$

where

$$\tilde{A}_k = \sum_{l=0}^{L} \mathrm{Re}\{\tilde{F}(s_{k+lN})\}, \tag{25a}$$

$$\tilde{B}_k = \sum_{l=0}^{L} \mathrm{Im}\{\tilde{F}(s_{k+lN})\}, \tag{25b}$$

$$W = \mathrm{e}^{2\pi\mathrm{i}/N}, \tag{25c}$$

$$s_m = \beta + 2\pi\mathrm{i}m/\tau_N, \tag{25d}$$

with the real constant $\beta = 6/\tau_N$ based upon experience and the recommendation of Durbin (1974). Evaluation of the bracketed terms in eqn (24) is accomplished through the use of the Fast Fourier Transform (Cooley and Tukey, 1965). In order to minimize the Gibbs phenomena near discontinuities, Lanczos σ factors are included (Lanczos, 1956).

Notice that from eqns (24) and (25), the determination of $F(\tau_n)$ for $n = 0, 1, \ldots, N-1$ depends upon the values of $\tilde{F}(s_m)$ for $m = 0, 1, \ldots, M-1$ where $M = N(L+1)$. Consequently, the boundary integral equations

$$C_{\alpha\beta}(\xi)\tilde{u}_\alpha(\xi, s_m) = \int_S [\tilde{G}^*_{\alpha\beta}(x, \xi; s_m)\tilde{t}_\alpha(x, s_m) - \tilde{F}^*_{\alpha\beta}(x, \xi; s_m)\tilde{u}_\alpha(x, s_m)]\, \mathrm{d}S(x) \tag{26}$$

must be solved independently at each of the M discrete values s_m of the transform

parameters. In the current implementation, $L = 0$ to minimize the computational effort for a given number of output time steps N. However, additional accuracy can be obtained for the numerical inversion by increasing L.

In order to solve eqn (26) for the unknown generalized displacements and tractions, some form of spatial discretization must be introduced. Quadratic boundary elements are utilized to describe the geometry of the surface, while $\tilde{u}_\alpha$ and $\tilde{t}_\alpha$ may have a linear, quadratic, or quartic variation specified within each element. A fully conforming approach is taken in order to maintain interelement continuity of generalized displacements. However, applied generalized tractions may be discontinuous.

Spatial collocation is then used to develop a system of algebraic equations. In the process, the discretized form of eqn (26) is written at each functional node. The integration is performed numerically by invoking self-adaptive schemes to ensure both accuracy and efficiency. Strongly singular blocks of $F_{\alpha\beta}$ identified in eqns (19) are evaluated indirectly with a generalization of the rigid body technique (Cruse, 1974; Dargush and Banerjee, 1989a). The resulting system of equations can be written in matrix form

$$[G^m]\{t^m\} = [F^m]\{u^m\} \tag{27}$$

or finally, after applying the specified boundary conditions,

$$[A^m]\{x^m\} = \{b^m\}, \tag{28}$$

where $[A^m]$ is a square, nonsymmetric complex matrix and once again $m = 0, 1, \ldots, M-1$. After all of the vectors $\{x^m\}$ are determined, the desired time-domain solutions are synthesized by employing the FLIT algorithm defined in eqn (24).

Finally, it should be noted that since this entire dynamic poroelastic/thermoelastic formulation was implemented in the general purpose code, GPBEST, a wide range of additional facilities is available, including multiple material regions, sliding interfaces, displacement discontinuities, and convection boundary conditions. However, the numerical applications considered below are intended to illustrate some of the basic phenomena associated with the dynamic theories. More elaborate applications will be examined elsewhere.

POROELASTIC APPLICATIONS

Transient load on surface of half-space

The first problem addressed concerns plane strain step loading applied uniformly to the surface of a half-space. Simon *et al.* (1984) presented a solution for the same problem where the materials are dynamically compatible. The loading boundary conditions for this test problem include a step total stress, $\sigma = \sigma_0 H(t)$, and free fluid flow, $p = 0$, at the top surface of the half-space.

A representative strip, one unit wide and ten units deep, is isolated for the boundary element analysis and discretized with a total of fifty quadratic surface elements. The depth is sufficient to ensure that no waves are reflected by the lower boundary within the solution times of interest. Alternatively, enclosing elements could be employed (Ahmad and Banerjee, 1988).

For the three kinds of dynamically compatible material considered in this example, the reader is referred to Simon *et al.* (1984). Nondimensional material parameters are defined by

$$\lambda^* = \frac{\lambda}{\lambda + 2\mu + \alpha^2 Q},$$

$$\mu^* = \frac{\mu}{\lambda + 2\mu + \alpha^2 Q},$$

$$Q^* = \frac{Q}{\lambda + 2\mu + \alpha^2 Q},$$

$$\rho^* = 1,$$

$$\rho_f^* = \frac{\rho_f}{\rho},$$

$$m^* = \frac{m}{\rho},$$

$$\kappa^* = 1,$$

and set as follows: material No. 1 $\kappa^* = 1.0$ $\lambda^* = 0.006751$ $\mu^* = 0.01013$ $Q^* = 0.973$ $\rho^* = 1.0$ $\rho_f^* = 0.973$ $n = 0.333$ $\alpha = 1.0$; material No. 2 $\kappa^* = 1.0$ $\lambda^* = 0.0878$ $\mu^* = 0.1317$ $Q^* = 1.459$ $\rho^* = 1.0$ $\rho_f^* = 0.973$ $n = 0.333$ $\alpha = 0.667$; material No. 3 $\kappa^* = 1.0$ $\lambda^* = 0.169$ $\mu^* = 0.2535$ $Q^* = 2.922$ $\rho^* = 1.0$ $\rho_f^* = 0.973$ $n = 0.333$ $\alpha = 0.333$.

No shear waves exist for this one-dimensional problem. However, waves of the first and second kind are present (i.e. two dilatational waves). The faster waves of the first kind are an undamped disturbance traveling at nondimensional speed v_1, and the slower waves of the second kind are a damped disturbance traveling at nondimensional speed v_2. The propagation speeds of the two dilatation waves are summarized as: material No. 1 $v_1 = 1$, $v_2 = 0.1153$; material No. 2 $v_1 = 1$, $v_2 = 0.5092$; material No. 3 $v_1 = 1$, $v_2 = 1$.

The displacements of the solid at the surface are shown in Fig. 1 plotted against the time parameter $\tau = t/(\rho\kappa)$ for the three material cases (No. 1, No. 2, and No. 3). Nondimensional scale for displacements is used, i.e. $uV_c/(\kappa\sigma_0)$, where $V_c = \sqrt{(\lambda + 2\mu + \alpha^2 Q)/\rho}$. The plots for the surface displacement suggest a 'creep' effect due to losses associated with relative fluid motion. (The displacement response in a single-phase elastic medium is linear with time.) Figure 2(a) shows the pore pressure at a depth $\xi = 1.0$ versus τ for material No. 2, while the total stress at that location is plotted in Fig. 2(b). Very good agreement is observed between BEM and analytical solutions. In particular, the arrival of the two waves is captured quite well, as indicated in Fig. 2(a).

Explosion in a spherical cavity

For the second example, consider an infinite three-dimensional poroelastic medium containing a spherical cavity of radius R. (The corresponding two-dimensional cylindrical cavity response is studied in detail in Chen, 1992). Nondimensional spatial and temporal scales are introduced by defining $\xi = r/R$ and $\tau = t(\mu/\rho)^{1/2}/R$, respectively. The poroelastic

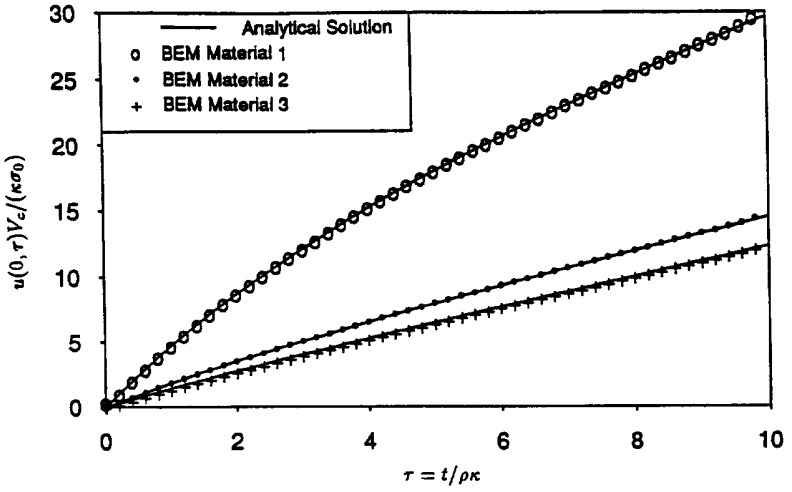

Fig. 1. Transient load on surface of half-space– surface displacement.

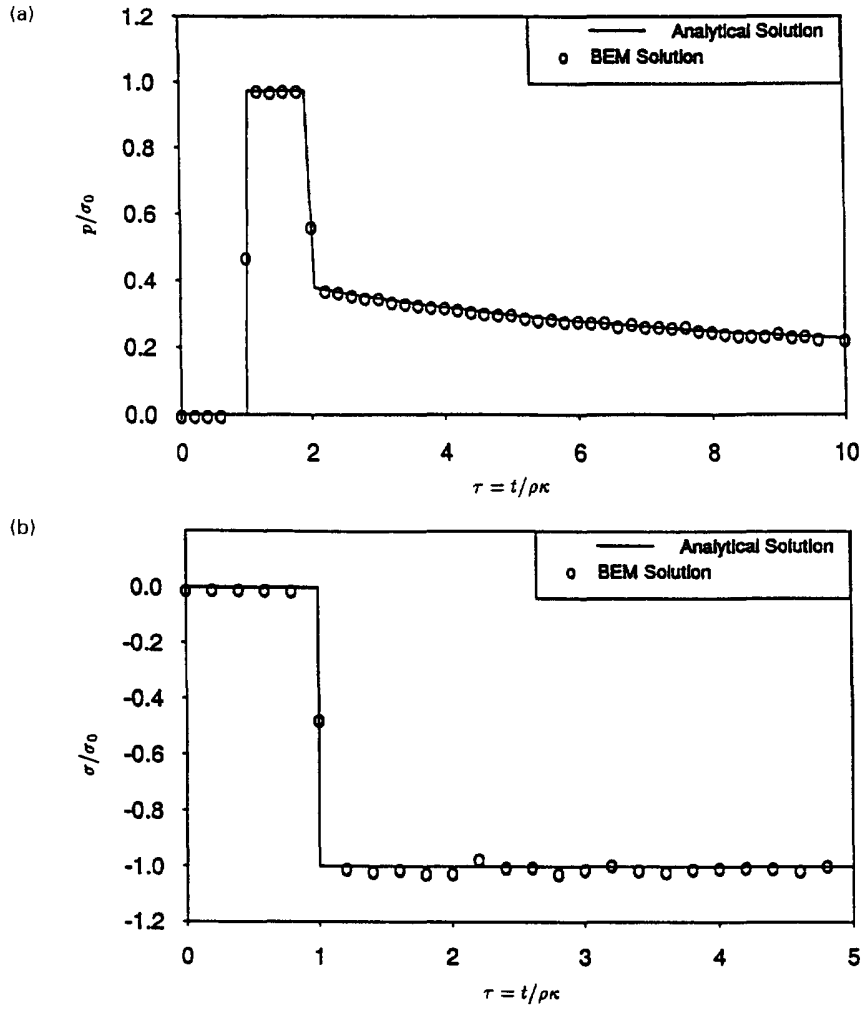

Fig. 2. Transient load on surface of half-space—response for material No. 2. (a) Pore pressure, (b) total stress.

material properties are also nondimensionalized, and specified as follows: $\mu^* = 1$, $\lambda^* = 2$, $\rho^* = 1$, $\rho_f^* = 0.5$, $Q^* = 23$, $m^* = 1.25$, $b^* = 16$, $\alpha = 0.984$ with $\lambda^* = \lambda/\mu$, $\rho_f^* = \rho_f/\rho$, $Q^* = Q/\mu, m^* = \rho_f^*/n$, and $b^* = \eta R/(k^2\rho\mu)^{1/2}$. The cavity surface is subjected to a uniform pressure, p_0, applied suddenly at time zero and subsequently maintained at that level.

In the boundary element analysis of this problem, discretization is required for only the surface of the cavity. Additionally, due to symmetry, modeling can be confined to just the positive octant of that surface. Two levels of mesh refinement are considered, involving three and twelve nine-noded Lagrangian elements, respectively. Analysis is conducted for nondimensional time steps $\Delta\tau = 0.2$ and $\Delta\tau = 0.1$ in order to investigate convergence characteristics. In each case, fifty values of the transform parameter are utilized, and a permeable cavity surface is assumed. The resulting radial displacement of the cavity surface at $\xi = 1$ is plotted versus time in Fig. 3. It is evident that very good convergence has been obtained, and that even a simple three-element model produces the proper response.

Comparison of the poroelastic behavior with that of a single-phase elastic medium is presented in Fig. 4. Results for both permeable and impermeable hydraulic boundaries are included. The properties for the elastic media are taken to correspond to the fully drained case. Thus, $\mu^* = 1$, $\lambda^* = 2$, and $\rho^* = 1$. The required elastic kernel functions are well known (Eringen and Suhubi, 1975), but can also be obtained as a limiting form of the present poroelastic kernels (Chen, 1992). Since an analytical solution is available for the elastic

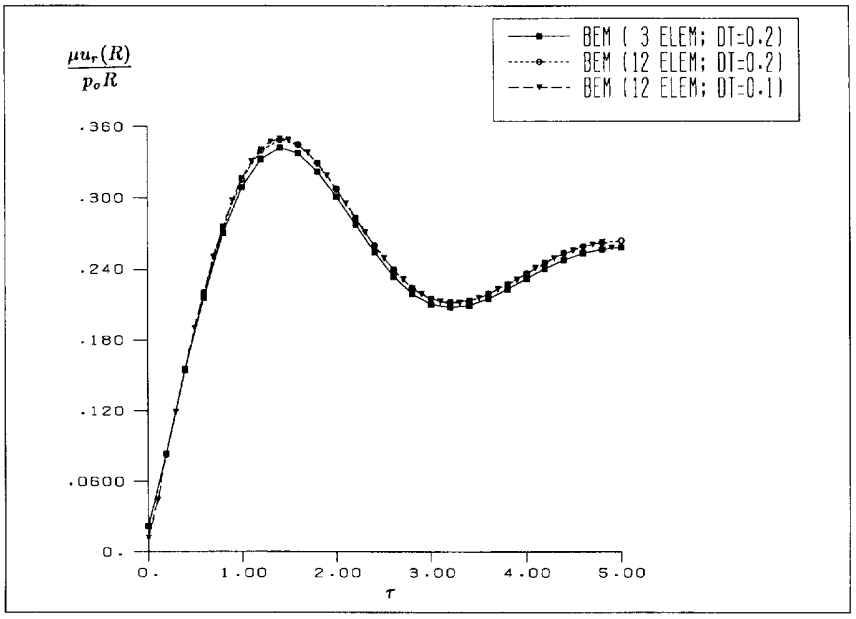

Fig. 3. Explosion in a spherical cavity—convergence study for cavity surface displacement.

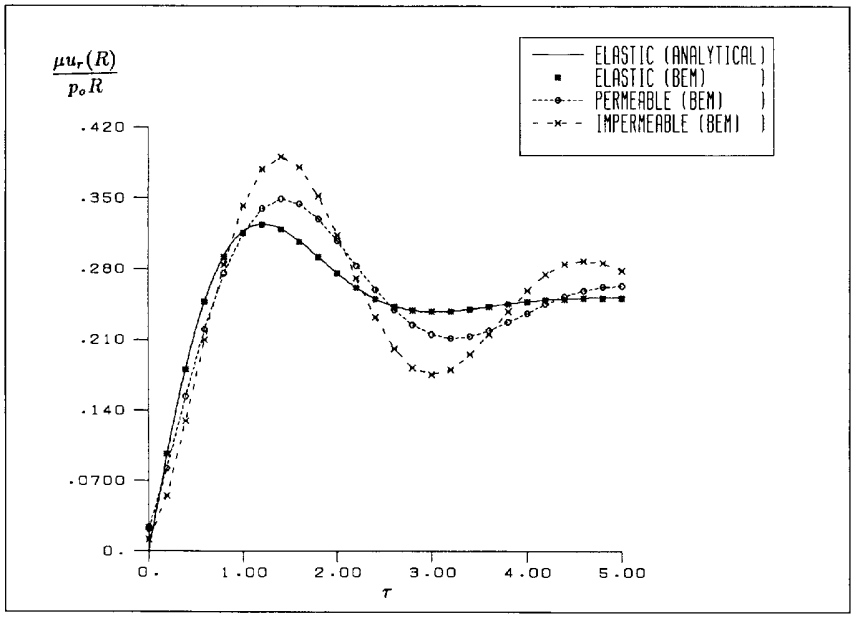

Fig. 4. Explosion in a spherical cavity—cavity surface displacement under permeable and impermeable conditions.

case, this is also shown in Fig. 4 to illustrate the accuracy of the underlying boundary element methodology. All three of the BEM response curves were obtained for the twelve-element model with $\Delta\tau = 0.2$. It is evident from the figure that while the general shape of the time-history response is similar for both the poroelastic and elastic media, the peak displacements are significantly greater in the two-phase material, particularly when the surface of the cavity is impermeable. Notice also that the peak is somewhat delayed compared to the single-phase elastic response.

Vertical impedance of a square footing

The final poroelastic application involves a time-harmonic analysis of a rigid, smooth, massless square plate with length dimension $2a$ vibrating on the surface of a poroelastic

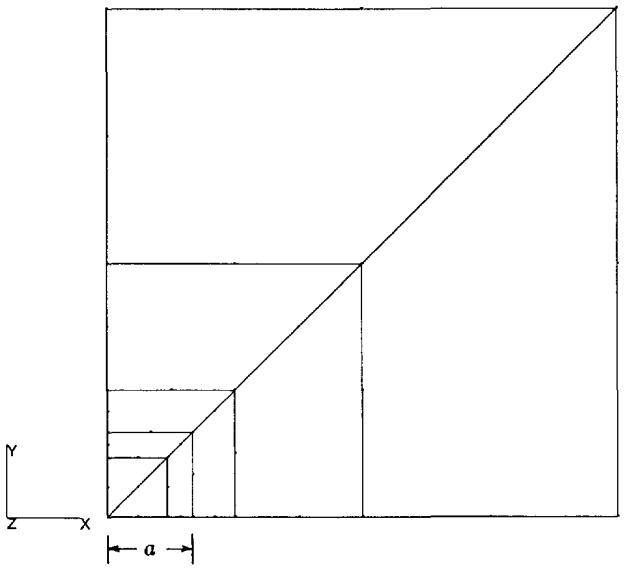

Fig. 5. Vertical impedance of a square footing—boundary element model.

half-space. Once again dimensionless spatial and temporal scales are introduced such that $x_i^* = x_i/a$ and $a_0^* = \omega a\,(\rho/\mu)^{1/2}$, where ω is the circular frequency of the plate vibration. The nondimensional material properties of the poroelastic medium are $\mu^* = 1$, $\lambda^* = 2$, $\rho^* = 1$, $\rho_f^* = 0.4$, $Q^* = 10$, $k^* = 1.0$, $\eta^* = 1.0$, $n = 0.3$, and $\alpha = 0.9$. The corresponding elastic case has been investigated by Wong and Luco (1976) and Ahmad (1986).

Figure 5 depicts the boundary element model employed for the analysis with quarter symmetry assumed. A total of ten elements are used, all on the surface of the half-space, which is assumed to be permeable. A unit vertical displacement amplitude is applied over the surface of the plate, and the problem is solved for a range of frequencies. At each frequency, the resulting vertical tractions under the plate are integrated numerically to determine the vertical impedance of the footing. Results for the real and imaginary components of the impedance are shown in Fig. 6. Values obtained, using both quadratic and quartic functional variation within each element, are provided. Excellent convergence is evident at lower frequencies, while some differences appear at the higher end, due primarily to the crudeness of the quadratic representation.

The quartic element model is then used to examine the effects of soil permeability. Four values of k^* ranging from 0.01 to 10,000. were examined with the real and imaginary impedances provided in Fig. 7. From these curves, it is clear that permeability can have a significant impact on the response. A more detailed parametric study of the square footing, along with other typical foundation designs, is currently underway.

THERMOELASTIC APPLICATION

Half-space subjected to a step surface heating

As an illustrative numerical example of dynamic thermoelasticity, we consider the first Danilovskaya (1950) problem of classical thermoelasticity. A half-space ($x > 0$), with boundary $x = 0$ is assumed initially to be at rest and to have zero temperature. At time $t = 0^+$, the traction-free boundary of the half-space is subjected to a step temperature $\theta_0 H(t)$, which remains constant thereafter. It is convenient to introduce the usual dimensionless variables as follows:

$$\xi_i = \frac{x_i}{a} \quad \tilde{T} = \frac{T}{\theta_0} \quad \tau = \frac{\kappa}{\rho c}\frac{t}{a^2} \quad \tilde{\sigma}_{ij} = \frac{\sigma_{ij}}{\gamma_t \theta_0} \quad \tilde{u}_i = \frac{(\lambda+2\mu)u_i}{a\gamma_t\theta_0},$$

where

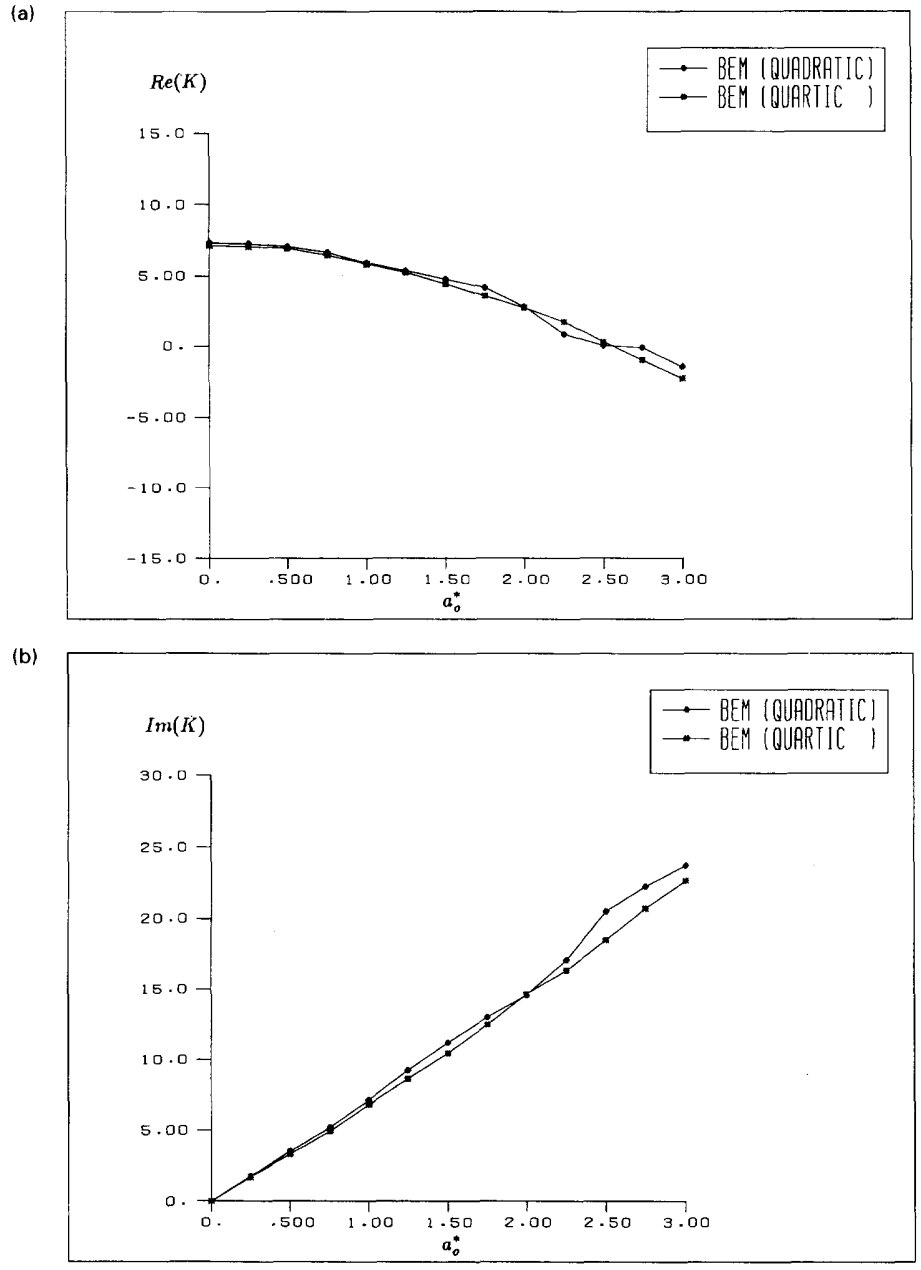

Fig. 6. Vertical impedance of a square footing—convergence study. (a) Real component of impedance, (b) imaginary component of impedance.

$$a = \frac{1}{c_s}\frac{\kappa}{\rho c} \quad c_s = \sqrt{\frac{\lambda+2\mu}{\rho}}.$$

As proposed in Boley and Weiner (1960), the thermomechanical coupling parameter is

$$\delta = \frac{\gamma_t^2 T_0}{\rho c\,(\lambda+2\mu)}.$$

All calculations reported were performed with the material constants selected as follows:

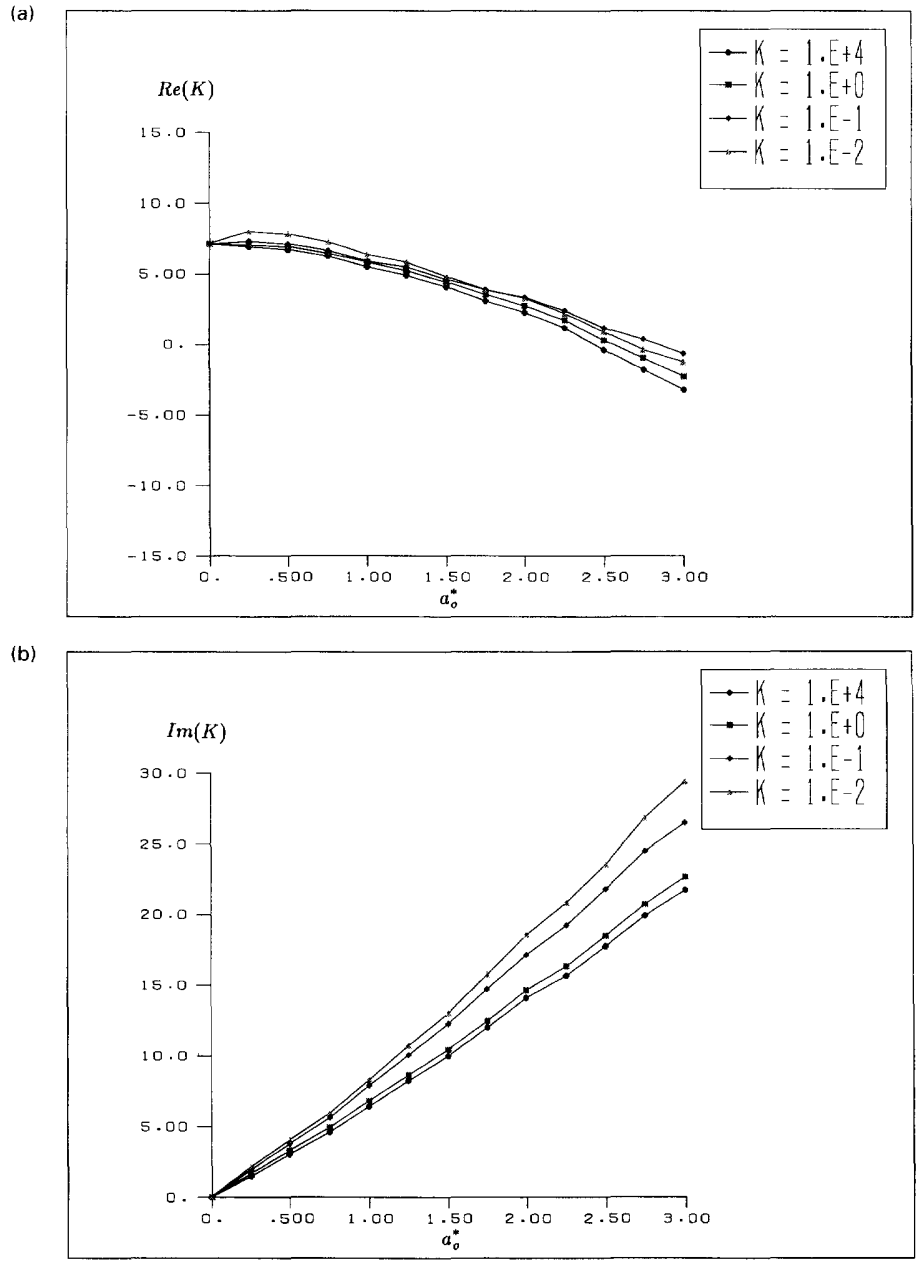

Fig. 7. Vertical impedance of a square footing—effects of soil permeability. (a) Real component of impedance, (b) imaginary component of impedance.

$$\beta = 3.34 \times 10^4 \,\mathrm{kg\,K^{-1}\,cm^{-1}\,s^{-2}},$$

$$\lambda + 2\mu = 1.99 \times 10^9 \,\mathrm{kg\,cm^{-1}\,s^{-2}},$$

$$\rho = 7.82 \times 10^{-3} \,\mathrm{kg\,cm^{-3}},$$

$$c = 4.61 \times 10^6 \,\mathrm{cm^2\,K^{-1}\,s^{-3}},$$

$$\kappa = 1.70 \times 10^3 \,\mathrm{kg\,cm\,K^{-1}\,s^{-3}},$$

to correspond to the properties of stainless steel. The boundary element representation of the problem geometry is identical to that utilized in the first poroelastic example.

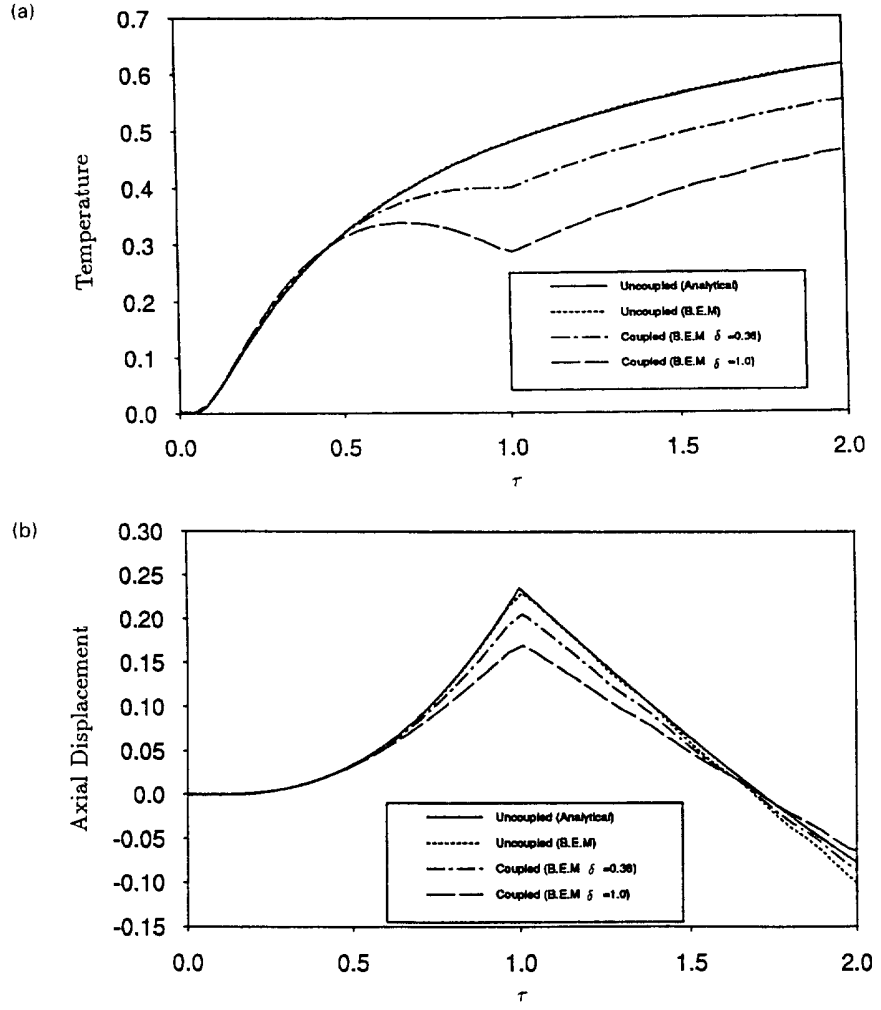

Fig. 8. Half-space subjected to a step surface heating (classical theory). (a) Temperature response, (b) displacement response.

Figure 8 depicts the time histories of the dimensionless temperature and displacement at a particular point. The point chosen, $\xi = 1.0$, is the location of the elastic wave front at the nondimensional time $\tau = 1.0$. In these figures the analytical solutions for the uncoupled problem obtained by Sternberg and Chakravorty (1959) via Laplace transform are also presented. The present BEM solution shows good agreement with the analytical result. An analytical solution for the coupled problem is unavailable in the literature. In these figures, the coupled results are presented for $\delta = 0.36$ and $\delta = 1.0$ for illustrative purposes only. These values are unrealistically high for the material of interest.

A point of interest is the distribution of temperature shown in Fig. 8. The effect of strong coupling is to accelerate thermal diffusion ahead of the wave front and decelerate it behind the front. This is so, since the conversion of thermal and mechanical energy is most likely to take place predominantly at or near the wave front. In fact, the BEM results obtained indicate that a negative temperature gradient is generated ahead of the wave for strong coupling. As can be inferred from the plots, the temperature distribution behind the wave front asymptotically approaches the uncoupled solution with increasing time.

Figures 9 and 10 provide the results for the same problem using L–S and G–L theories, respectively. In Fig. 9, the nondimensional relaxation time $\tau_0 = 2$. As a result, for the

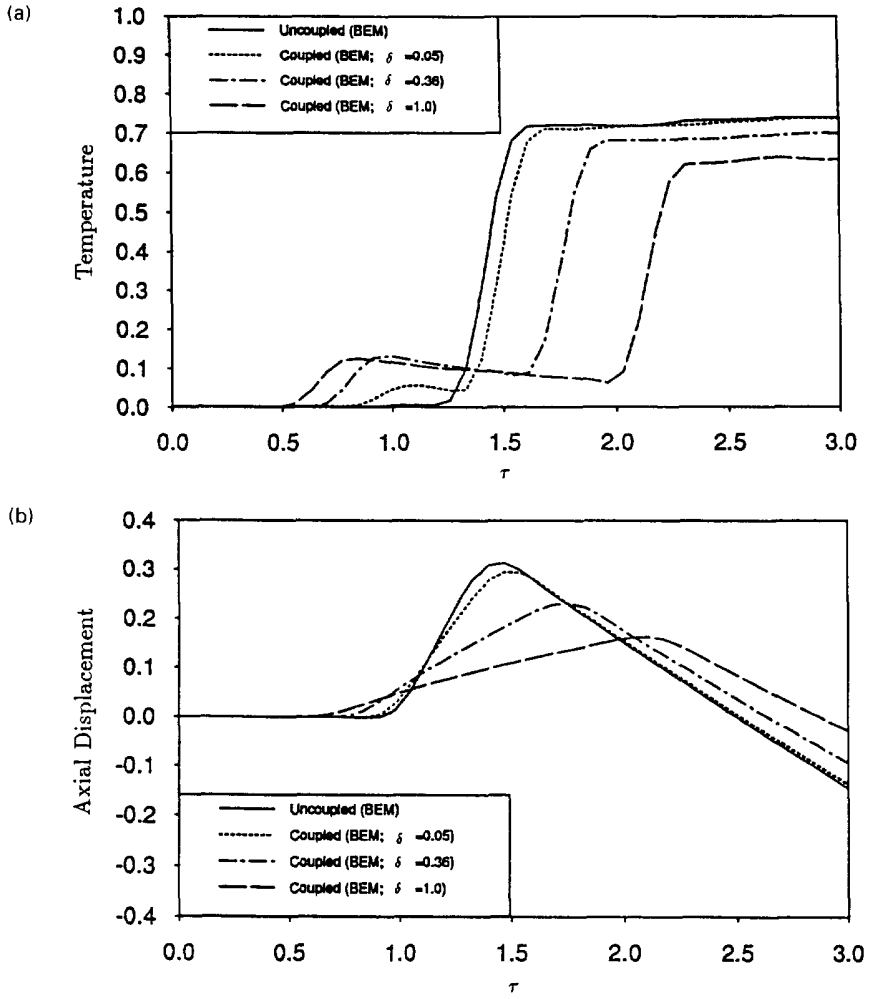

Fig. 9. Half-space subjected to a step surface heating (Lord–Shulman theory). (a) Temperature response, (b) displacement response.

uncoupled case, the elastic wave front propagates with a velocity equal to one and the thermal wave front propagates with a velocity of $1/\sqrt{2}$. Due to the one-way coupling, the fast elastic wave does not cause a sudden rise in temperature at its arrival time $\tau = 1.0$. However, we find that there are two dramatic changes in temperature in coupled cases due to the arrival of both the elastic and thermal waves. In all cases, the displacement response is much more gradual.

For the G–L theory analysis, the two relaxation times τ_1 and τ_2 were both set equal to a nondimensional value of 2.25. While the temperature response in Fig. 10(a) is quite similar to that obtained for the L–S theory, significant differences appear in the displacement time history. In particular, under G–L theory, sudden dramatic changes in displacement are associated with the arrival of the elastic and thermal waves. Clearly, the introduction of relaxation times in thermoelastic theories can significantly alter response.

For this example, nondimensional units were employed to establish the coupling and relaxation characteristics. While this is useful in distinguishing the various theories and in validating the implementations, it is also somewhat misleading. In particular, by introducing more realistic values for these parameters, one finds that the dynamic theory of thermoelasticity and second sound effects are important only under exceptional circumstances. For example, in a metal at room temperature, the characteristic times for heat conduction and elastic shear wave propagation can be written as

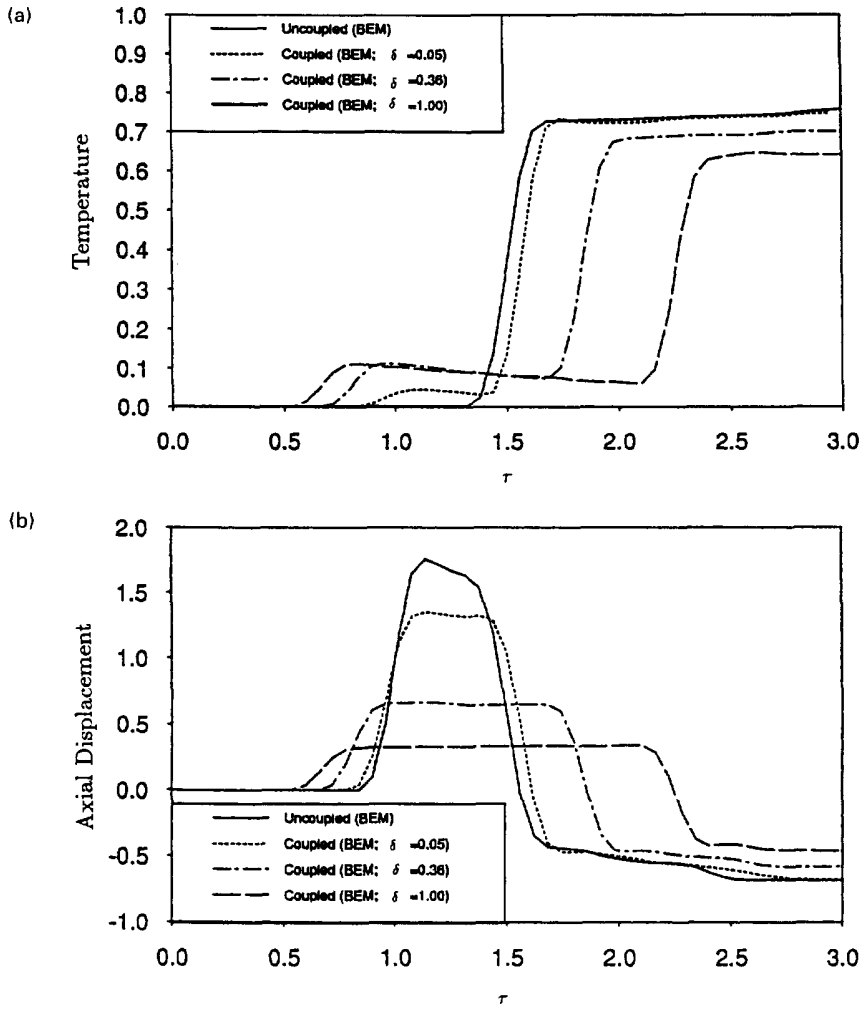

Fig. 10. Half-space subjected to a step surface heating (Green–Lindsay theory). (a) Temperature response, (b) displacement response.

$$\tau_h = \frac{\rho c L^2}{\kappa}$$

and

$$\tau_s = \left(\frac{\rho}{\mu}\right)^{1/2} L,$$

respectively. Those two times are comparable only over very small distances L of the order of 10^{-8} m. The corresponding time scale is measured in picoseconds. Consequently, for most applications the classical theory, along with a quasistatic approximation, is adequate. Boundary element methods for that theory have been presented previously (Dargush and Banerjee, 1989b; 1990).

However, it should be noted that second sound effects have been detected in solids at low temperatures. Furthermore, the dynamic theory considered here may have some significance in superconductors and for applications involving lasers with extremely short pulses. The latter situation was considered in some detail by Hector *et al.* (1992), in which

the authors examined the temperature distribution in a material modeled with a hyperbolic constitutive law subjected to irradiation by a mode-locked laser.

CONCLUSIONS

In the present work, the analogy between dynamic poroelasticity and generalized thermoelasticity was exploited for the development of a single boundary element formulation appropriate to both theories. The resulting formulation is applicable to transient and time-harmonic problems involving both two- and three-dimensional domains. The integral representation is derived directly from the governing differential equations in the Laplace domain. By utilizing the infinite space adjoint fundamental solution, a boundary-only formulation is obtained, thus eliminating the need for volume discretization for the analysis of piecewise homogeneous media, with zero body forces and initial conditions.

While the resulting integral equations are exact statements, both temporal and spatial discretization are required for the solution of practical problems. Two approaches are briefly discussed for the representation in time. In the first approach, the integral equations and kernel functions are transformed from the Laplace domain to the time domain. Although this method is computationally intensive at the kernel level, it does permit analysis of nonlinear phenomena. For the second approach, the equations are solved in the Laplace domain, and then the solutions are transformed to the time domain. Only this latter approach is implemented, since the interest here is limited to linear analysis. State-of-the-art boundary element methodology is employed for the spatial discretization and numerical integration in order to provide accurate solutions.

Numerical examples are used to validate the implementation and to explore the dynamic behavior of media governed by these theories. In all cases, detailed convergence studies establish the self-consistency of the methodology and provide the basis for mesh and time step selection. The poroelastic applications, particularly those involving the investigation of an underground explosion and the calculation of foundation impedances, indicate that the presence of an interstitial fluid can have a significant effect on the response. Additionally, in the thermoelastic application, BEM results correlate well with a known analytical solution. Further applications of the present boundary element method for both poroelasticity and thermoelasticity are currently underway.

REFERENCES

Ahmad, S. (1986). Linear and nonlinear dynamic analysis by boundary element method. PhD dissertation, State University of New York at Buffalo.

Ahmad, S. and Banerjee, P. K. (1988). Transient elastodynamic analysis of three dimensional problems by BEM. *Int. J. Num. Meth. Engng* **26,** 1560–1580.

Auriault, J. L., Borne, L. and Chambon, R. (1985). Dynamics of porous saturated media; checking of the generalized law of Darcy. *J. Acoust. Soc. Am.* **77,** 1641–1650.

Banerjee, P. K. and Ahmad, S. (1985). Advanced three-dimensional dynamic analysis by boundary element methods. In *Advanced Topics in Boundary Element Analysis* (Edited by T. A. Cruse, A. B. Pifko, and H. Armen), AMD-72, ASME, pp. 65–81.

Banerjee, P. K. and Butterfield, R. (1981). *Boundary Element Methods in Engineering Science.* McGraw-Hill, London.

Biot, M. A. (1956a). The theory of propagation of elastic waves in a fluid-saturated porous solid. I. Low frequency range. *J. Acoust. Soc. Am.* **28,** 168–178.

Biot, M. A. (1956b). The theory of propagation of elastic waves in a fluid-saturated porous solid. II. Higher frequency range. *J. Acoust. Soc. Am.* **28,** 179–191.

Biot, M. A. (1956c). Thermoelasticity and irreversible thermodynamics. *J. Appl. Phys.* **27,** 240–253.

Biot, M. A. (1962a). Mechanics of deformation and acoustic propagation in porous media. *J. Appl. Phys.* **33,** 1482–1498.

Biot, M. A. (1962b). Generalized theory of acoustic propagation in porous dissipative media. *J. Acoust. Soc. Am.* **34**(9), 1254–1264.

Boley, B. A. and Weiner, J. H. (1960). *Theory of Thermal Stresses.* John Wiley & Sons, New York.

Bonnet, G. (1987). Basic singular solutions for a poroelastic medium in the dynamic range. *J. Acoust. Soc. Am.* **82**(5), 1758–1762.

Boutin, C., Bonnet, G. and Bard, P. Y. (1987). Green functions and associated sources in infinite and stratified poroelastic media. *Geophys. J. Roy. Astr. Soc.* **90,** 521–550.

Bowen, R. M. (1982). Compressional porous media models by use of the theory of mixtures. *Int. J. Engng Sci.* **20,** 697–735.

Burridge, R. and Keller, J. B. (1981). Poroelasticity equations derived from microstructure. *J. Acoust. Soc. Am.*, **10,** 1140–1146.
Chadwick, P. (1960). Thermoelasticity. The dynamical theory. In *Progress in Solid Mechanics* (Edited by I. N. Sneddon and R. Hill), Vol. 1, pp. 265–328. North Holland, Amsterdam.
Chen, J. (1992). Fundamental solutions and boundary element formulations for dynamic problems of poroelasticity and thermoelasticity. PhD dissertation, State University of New York at Buffalo.
Cheng, A. H.-D. and Badmus, T. (1991). Integral equation for dynamic poroelasticity in frequency domain with BEM solution. *ASCE J. Engng Mech.* **117,** 1136–1158.
Cheng, A. H.-D. and Liggett, J. A. (1984). Boundary integral equation method for linear porous elasticity with applications to soil consolidation, *Int. J. Num. Meth. Engng.* **20,** 255–278.
Cleary, M. P. (1977). Fundamental solutions for a fluid-saturated porous solid. *Int. J. Solids Struct.* **13,** 785–806.
Cooley, J. W. and Tukey, J. W. (1965). An algorithm for machine calculation of complex Fourier series. *Math. Comp.*, **19,** 297–301.
Cruse, T. A. (1974). An improved boundary integral equation method for three-dimensional elastic stress analysis. *Comp. and Struct.*, **4,** 741–754.
Cruse, T. A. and Rizzo, F. J. (1968). A direct formulation and numerical solution of the general transient elastodynamic problem. I. *J. Math. Anal. Appl.* **22,** 244–259.
Danilovskaya, V. I. (1950). Thermal stresses in an elastic half-space due to a sudden heating of its boundary (in Russian). *Prikladnaya Matematika i Mekhanika* **14,** 316–318.
Dargush, G. F. (1987). Boundary element methods for the analogous problems of thermomechanics and soil consolidation. PhD dissertation, State University of New York at Buffalo.
Dargush, G. F. and Banerjee, P. K. (1989a). A time domain boundary element method for poroelasticity. *Int. J. Num. Meth. Engng.* **28,** 2423–2449.
Dargush, G. F. and Banerjee, P. K. (1989b). Development of a boundary element method for time dependent planar thermoelasticity. *Int. J. Solids Struct.*, **25,** 999–1021.
Dargush, G. F. and Banerjee, P. K. (1990). Boundary element methods in three-dimensional thermoelasticity. *Int. J. Solids Struct.* **26,** 199–216.
Dargush, G. F. and Banerjee, P. K. (1991). A boundary element method for axisymmetric soil consolidation. *Int. J. Solids Struct.* **28,** 897–915.
Dominguez, J. (1992). Boundary element approach for dynamic poroelastic problems. *Int. J. Num. Meth. Engng* **35,** 307–324.
Durbin, F. (1974). Numerical inversion of Laplace transforms: an efficient improvement to Dubner and Abate's method. *Computer J.*, **17,** 371–376.
Eringen, A. C. and Suhubi, E. (1975). *Elastodynamics.* Academic Press, New York.
Green, A. E. and Lindsay, K. E. (1972). Thermoelasticity. *J. Elasticity* **2,** 1–7.
Hector, L. G., Kim, W.-S. and Özisik, M. N. (1992). Hyperbolic heat conduction due to a mode locked laser pulse train. *Int. J. Engng Sci.* **30,** 1731–1744.
Ionescu-Cazimir, V. (1964). Problem of linear coupled thermoelasticity. Theorems on reciprocity for the dynamic problem of coupled thermoelasticity. I. *Bull. Acad. Polon., Ser. Sci. Techn.* **12,** 473–488.
Lanczos, C. (1956). *Applied Analysis.* Prentice-Hall, Englewood Cliffs, NJ.
Lord, H. W. and Shulman, Y. (1967). A generalized dynamical theory of thermoelasticity. *J. Mech Phys. Solids* **15,** 299–309.
Manolis, G. D. and Beskos, D. E. (1981). Dynamic stress concentration studies by boundary integrals and Laplace transform. *Int. J. Num. Meth. Engng* **17,** 573–599.
Manolis, G. D. and Beskos, D. E. (1989). Integral formulation and fundamental solutions of dynamic poroelasticity and thermoelasticity. *Acta Mechanica* **76,** 89–104.
Nishimura, N. and Kobayashi, S. (1989). A boundary integral equation method for consolidation problems. *Int. J. Solids Struct.* **25,** 1–21.
Norris, A. N. (1985). Radiation from a point source and scattering theory in a fluid-saturated porous solid, *J. Acoust. Soc. Am.* **77,** 2012–2023.
Nowacki, W. (1964). Green functions for the thermoelastic medium, I. *Bull. Acad. Polon., Ser. Sci. Techn.* **12,** 315–321.
Nowacki, W. (1975). *Dynamic Problems of Thermoelasticity.* Noordhoff Int. Publ., Leyden.
Nowacki, W. (1986). *Thermoelasticity.* Pergamon, Oxford.
Plona, T. J. (1980). Observation of a second bulk compressional wave in a porous medium at ultrasonic frequencies. *Appl. Phys. Lett.* **36,** 259–261.
Predeleanu, M. (1984). Development of boundary element method to dynamic problems for porous media. *Appl. Math. Modeling* **8,** 378–382.
Prevost, J. H. and Tao, D. (1983). Finite element analysis of dynamic coupled thermoelasticity problems with relaxation times. *J. Appl. Mech.* **50,** 817–822.
Simon, B. R., Zienkiewicz, O. C. and Paul, D. K. (1984). An analytical solution for the transient response of saturated porous elastic solids. *Int. J. Num. Anal. Meth. Geomech.* **8,** 381–398.
Sladek, V. and Sladek, J. (1984). Boundary integral equation method in thermoelasticity. Part I: General analysis. *Appl. Math. Modelling* **7,** 241–253.
Sternberg, E. and Chakravorty, J. G. (1959). On inertia effects in a transient thermoelastic problem. *J. Appl. Mech.* **26,** 503–509.
Vernotte, P. (1958). Les paradoxes de la theorie continue de l'equation de la chaleur. *C. Roy. Acad. Sci.* **246,** 3154–3155.
Wong, H. L. and Luco, J. E. (1976). Dynamic response of rigid foundations of arbitrary shape. *Earthquake Engng Struct. Dyn.* **4,** 579–587.
Zienkiewicz, O. C. and Shiomi, T. (1984). Dynamic behavior of saturated porous media; the generalized Biot formulation and its numerical solution. *Int. J. Num. Anal. Meth. Geomech.* **8,** 71–96.
Zienkiewicz, O. C., Chang, C. T. and Bettess, P. (1980). Drained, undrained, consolidating and dynamic behavior assumptions in soil. Limits of validity. *Geotechnique* **30,** 385–395.

APPENDIX: THREE-DIMENSIONAL KERNELS

The Appendix details the kernel functions $\tilde{G}^*_{\alpha\beta}$ and $\tilde{F}^*_{\alpha\beta}$ that appear in the boundary integral representation for dynamic poroelasticity and thermoelasticity. Latin subscripts vary from 1 to 3, while Greek subscripts assume values from 1 to 4.

Then, for the generalized displacement kernel,

$$\tilde{G}^*_{ij} = \frac{d_0}{r}[\delta_{ij}\,\mathrm{e}^{-\lambda_3 r}] + \frac{d_1}{r^3}[-\{a_{ij}(1+\lambda_1 r)+b_{ij}(\lambda_1^2 r^2)\}c_2\,\mathrm{e}^{-\lambda_1 r} + \{a_{ij}(1+\lambda_2 r)+b_{ij}(\lambda_2^2 r^2)\}c_1\,\mathrm{e}^{-\lambda_2 r}$$

$$-\{a_{ij}(1+\lambda_3 r)+b_{ij}(\lambda_3^2 r^2)\}\,\mathrm{e}^{-\lambda_3 r}]$$

$$\tilde{G}^*_{4j} = \frac{d_2}{r^2}[-\{z_j(1+\lambda_1 r)\}\,\mathrm{e}^{-\lambda_1 r} + \{z_j(1+\lambda_2 r)\}\,\mathrm{e}^{-\lambda_2 r}]$$

$$\tilde{G}^*_{i4} = -\frac{d_3}{d_2}\tilde{G}^*_{4i}$$

$$\tilde{G}^*_{44} = \frac{d_4}{r}[-c_1\,\mathrm{e}^{-\lambda_1 r} + c_2\,\mathrm{e}^{-\lambda_2 r}],$$

where

$$y_i = x_i - \xi_i \quad r^2 = y_i y_i \qquad z_i = y_i/r$$

$$\kappa_1^2 = \frac{\rho_1 s^2}{\lambda+2\mu} \qquad \lambda_3^2 = \frac{\rho_1 s^2}{\mu}$$

$$\lambda_1^2+\lambda_2^2 = \kappa_1^2 + \frac{s}{M\zeta} + \frac{\alpha_1\alpha_2 s}{\zeta(\lambda+2\mu)} \quad \lambda_1^2\lambda_2^2 = \kappa_1^2\frac{s}{M\zeta}$$

$$d_0 = \frac{1}{4\pi\mu} \quad d_1 = \frac{1}{4\pi\rho_1 s^2} \qquad d_2 = \frac{\alpha_1}{4\pi(\lambda+2\mu)\zeta(\lambda_1^2-\lambda_2^2)}$$

$$d_3 = \left(\frac{\alpha_2 s}{\alpha_1}\right)d_2 \qquad d_4 = \frac{1}{4\pi\zeta}$$

$$c_1 = \left(\frac{\kappa_1^2-\lambda_1^2}{\lambda_2^2-\lambda_1^2}\right) \qquad c_2 = \left(\frac{\kappa_1^2-\lambda_2^2}{\lambda_2^2-\lambda_1^2}\right)$$

$$a_{ij} = 3z_i z_j - \delta_{ij} \qquad b_{ij} = z_i z_j.$$

Meanwhile, the generalized traction kernel can be written

$$\tilde{F}^*_{i\beta} = [(\lambda\tilde{G}^*_{k\beta,k} - \alpha T_0 s\tilde{G}^*_{4\beta})n_i + \mu(\tilde{G}^*_{i\beta,k} + \tilde{G}^*_{k\beta,i})n_k]$$

$$\tilde{F}^*_{4\beta} = -\zeta(\tilde{G}^*_{4\beta,k} + \rho_f s\tilde{G}^*_{k\beta})n_k$$

with n_i representing the unit outer normal. The explicit form of the derivatives are defined as follows:

$$\tilde{G}^*_{ij,k} = -\frac{d_0}{r^2}[q_{ijk}(1+\lambda_3 r)\,\mathrm{e}^{-\lambda_3 r}] - \frac{d_1}{r^4}[-\{g_{ijk}(1+\lambda_1 r)+h_{ijk}(\lambda_1^2 r^2)+p_{ijk}(\lambda_1^3 r^3)\}c_2\,\mathrm{e}^{-\lambda_1 r} + \{g_{ijk}(1+\lambda_2 r)$$

$$+h_{ijk}(\lambda_2^2 r^2)+p_{ijk}(\lambda_2^3 r^3)\}c_1\,\mathrm{e}^{-\lambda_2 r} - \{g_{ijk}(1+\lambda_3 r)+h_{ijk}(\lambda_3^2 r^2)+p_{ijk}(\lambda_3^3 r^3)\}\,\mathrm{e}^{-\lambda_3 r}]$$

$$\tilde{G}^*_{4j,k} = -\frac{d_2}{r^3}[-\{a_{jk}(1+\lambda_1 r)+b_{jk}(\lambda_1^2 r^2)\}\,\mathrm{e}^{-\lambda_1 r} + \{a_{jk}(1+\lambda_2 r)+b_{jk}(\lambda_2^2 r^2)\}\,\mathrm{e}^{-\lambda_2 r}]$$

$$\tilde{G}^*_{i4,k} = -\frac{d_3}{d_2}\tilde{G}^*_{4i,k}$$

$$\tilde{G}^*_{44,k} = -\frac{d_4}{r^2}[-\{z_k(1+\lambda_1 r)\}c_1\,\mathrm{e}^{-\lambda_1 r} + \{z_k(1+\lambda_2 r)\}c_2\,\mathrm{e}^{-\lambda_2 r}]$$

in which

$$g_{ijk} = 15z_i z_j z_k - 3z_i\delta_{jk} - 3z_j\delta_{ki} - 3z_k\delta_{ij}$$

$$h_{ijk} = -z_i\delta_{jk} - z_j\delta_{ki} - z_k\delta_{ij} + 6z_i z_j z_k$$

$$p_{ijk} = z_i z_j z_k$$

$$q_{ijk} = z_k\delta_{ij}.$$

The corresponding two-dimensional kernels can be found in Chen (1992).